Journal of Liquid Chromatography and Gas Chromatography, Europe
https://technicalreport.org/lcgceu/

LC GC Eu., Vol. 39, No.1, 01-06, 2026

Technical Reports Press

RESEARCH ARTICLE

Electronic Determinants of Cytotoxic Potency in Pyrazolo[1,5-*a*]pyridine–1,3,4-oxadiazole Chalcones

Benjamin Scott[1*]

[1] *Institute for Environmental Analysis Greenfield University United States*
[*] *Corresponding author*

Corresponding author:
banjamin_chemist@gmail.com

Received: 16 August 2025
Accepted: 20 November 2025
Available online: 30 March 2026

Abstract

The class of pyrazolo $[1,5-a]$ pyridine–1,3,4-oxadiazole chalcones features a fused heterocycle aromatic ring system, an oxadiazole moiety as a linker, and an electronically tailorable α,β-unsaturated carbonyl group. In this study, we sought to examine whether the anticancer effectiveness of 11a–j compounds depends on aryl substituents' electronics instead of merely on their lowest IC_{50} order. The cytotoxicity matrix for MCF-7, A549, Colo-205, and A2780 was first converted into pIC_{50} parameters. Then, aryl patterns were coded in terms of the summed Hammett constant ($\Sigma\sigma$). Relative potency scores were estimated against etoposide and related to mechanism-discriminating laboratory experiments. For the whole set of ten compounds, a very strong positive correlation of $\Sigma\sigma$ with the mean value of pIC_{50} was detected both through Pearson's r ($r = 0.873$; $p = 9.84 \times 10^{-4}$) and Spearman's ρ ($\rho = 0.796$; $p = 5.84 \times 10^{-3}$). One-electronic descriptor accounted for 76.2% of variance in pIC_{50} scores within compounds. A similar trend persisted for each cell line individually: MCF-7, A549, Colo-205, A2780. Compound 11j appeared the most effective in particular, among A549. Yet, its high potency comes along with dinitro substitution that requires further validation of selectivity, redox, and target-binding.

Keywords: chalcone; pyrazolo[1,5-*a*]pyridine; oxadiazole; anticancer; QSAR; DFT; Hammett analysis; molecular docking; MTT assay; cytotoxicity.

1. Introduction

The chalcones have been studied extensively in medicinal chemistry due to their capacity to induce diverse biological activities, including redox disturbance, alteration of signaling cascades, interference with tubulin polymerization, and interaction with DNA damage-response enzymes [1, 2, 3]. Such versatility presents challenges with respect to interpreting activity trends in chalcones. It could result from selective targeting of a single biological process, electronically activated Michael addition reactions, redox imbalance, assay-induced oxidative or electrophilic stress, or other means. Therefore, any anticancer potential should be assessed in the context of activity, potency, selectivity, and mechanism-consistent assays.

In this regard, the series of pyrazolo[1,5-*a*]pyridine–1,3,4-oxadiazole chalcones by Alapati *et al.* serves as an ideal case study [4]. Its design entails the integration of pyrazolo[1,5-*a*]pyridine and 1,3,4-oxadiazole moieties into a heteroaromatic system along with aryl-substituted chalcones. Ten new compounds 11a–j were synthesized, characterized with NMR and HRMS, and tested with MTT assay in MCF-7 breast cancer, A549 lung cancer, Colo-205 colon cancer, and A2780 ovarian cancer cells with etoposide serving as a positive control [4]. As a consequence, the activity matrix reveals 11j as the most potent analogue and suggests that 11a, 11b, 11g, 11i, and 11j have higher activity compared to etoposide against specific cell lines. From a chemical point of view, the next logical step would be to determine the key factor underlying the activity trend – substitution pattern, recognition motif, or generalized cytotoxic liability.

An assessment of electronic activity is warranted given the established connection between potency and enone reactivity. Electron-withdrawing substituents are expected to lower acceptor energy and enhance electrophilicity, whereas the opposite applies for electron-donating groups. Additionally, the electronic effect can drive a shift in the target profile. A variety of methods allows quantifying the extent of electronic activation. They include Hammett descriptors

Cite as: B. Scott (2026). Electronic Determinants of Cytotoxic Potency in Pyrazolo[1,5-*a*]pyridine–1,3,4-oxadiazole Chalcones. LC GC Eu., 39(1) (2026) 01-06.

[5, 6], DFT-based frontier orbitals [7, 8, 9], and QSAR with a limited set of electronic features. A distinction between broad-activity and lineage-specific compounds will also help differentiate cytotoxicity from selectivity. In particular, the most potent compound contains two nitro groups, which might indicate additional redox activity and normal-cell cytotoxicity [10, 11].

This paper makes four unique contributions. First, IC_{50} activity values are transformed to pIC_{50} to facilitate quantitative analysis. Second, a single-descriptor Hammett QSAR avoids overfitting in the limited series while addressing an interpretable chemical hypothesis. Third, fold-potency analysis distinguishes potency from superior performance relative to etoposide. Fourth, a comprehensive suite of assays will elucidate whether the observed structure–activity trend reflects electrophilic stress, redox reactivity, tubulin interference, or nonspecific cytotoxicity. Ultimately, the prioritized compounds and analogues provide a solid starting point for developing a mechanism-based chalcone scaffold.

2. Materials and Methods

This study uses the activity data reported by Alapati *et al.* for ten pyrazolo[1,5-*a*]pyridine–1,3,4-oxadiazole chalcone analogues 11a-j [4]. All these analogues contain a heteroaromatic and oxadiazole scaffold with a substituted phenyl ring on the position conjugated to the chalcone carbonyl moiety. The analogues were prepared via Suzuki coupling, iodination, Suzuki coupling, formation of nicotinaldehyde from substituted pyrazolo[1,5-*a*]pyridine derivatives, and Claisen condensation. The biological readout used was the half-maximal inhibitory concentration, IC_{50}, against the cancer cells.

First, the IC_{50} values were recorded as micromolar concentrations. Entries described as inactive, not determined, and empty were omitted from the analysis. For all compounds and active cell lines, the activity was then transformed to pIC_{50} as follows:

$$\mathrm{pIC}_{50,i,c} = 6 - \log_{10}\left(\mathrm{IC}^{\mu\mathrm{M}}_{50,i,c}\right), \tag{1}$$

where $\mathrm{IC}^{\mu\mathrm{M}}_{50,i,c}$ denotes the IC_{50} in micromolars of compound i against cell line c. Eq. (1) is equivalent to the commonly used $-\log_{10}(\mathrm{IC}_{50})$ and provides a normalized measure of potency proportional to ligand-target interaction energy. The average transformed potency over the active cell lines served as the principal activity measure of each compound:

$$\overline{\mathrm{pIC}}_{50,i} = \frac{1}{n_i}\sum_{c=1}^{n_i} \mathrm{pIC}_{50,i,c}, \tag{2}$$

where n_i is the number of cell lines against which compound i was active. Finally, a descriptive standard deviation of $pIC_{50,i,c}$ values allowed identifying broadly active versus lineage-specific analogues. Fold comparison of potency was conducted with the original IC_{50} values, although it can also be based on transformed activity according to the following relation:

$$\mathrm{Fold}_{a/b,c} = \frac{\mathrm{IC}_{50,b,c}}{\mathrm{IC}_{50,a,c}} = 10^{\left(\mathrm{pIC}_{50,a,c} - \mathrm{pIC}_{50,b,c}\right)}. \tag{3}$$

The assay concentrations were 0.5, 1, and 2 μmol/L. Consequently, IC_{50} values greater than 2 μmol/L need to be carefully analyzed because they might reflect the extrapolation of a sigmoidal curve beyond the tested concentration range. The primary analysis included the tabulated data regardless of whether the estimation was beyond fully bracketed points, whereas mechanistic interpretation paid attention to sub-μmol/L activity exclusively. If dose–response absorbance or viability data were available, they could serve for proper re-estimation of the IC_{50} values, which should not exceed 2 μmol/L or $pIC_{50} < 5.699$. A one-descriptor Hammett QSAR was developed to explore the association between the potency and degree of electronic activation. The substituted phenyl group conjugated with the chalcone carbonyl moiety is considered a key contributor to activity, thus, approximate Hammett constant was assigned to its substituents: $\sigma_p(\mathrm{OMe}) = -0.27$, $\sigma_m(\mathrm{OMe}) = 0.12$, $\sigma_p(\mathrm{Me}) = -0.17$, $\sigma_m(\mathrm{Me}) = -0.07$, $\sigma_p(\mathrm{NMe_2}) = -0.83$, $\sigma_p(\mathrm{Cl}) = 0.23$, $\sigma_p(\mathrm{Br}) = 0.23$, $\sigma_p(\mathrm{NO_2}) = 0.78$, and $\sigma_m(\mathrm{NO_2}) = 0.71$ [5, 6]. The sum of substituent constants was used to calculate the overall electronic effect:

$$\sigma_{\Sigma,i} = \sum_{k=1}^{m_i} \sigma_k, \tag{4}$$

where m_i is the number of substituents on the phenyl ring of the i-th compound. In this way, the most electron withdrawing analogue 11j was coded as $11\mathrm{j} = 2\sigma_p(\mathrm{NO_2}) = 1.42$. In turn, the least activating 11a had the descriptor value $\sigma_{\Sigma,a} = 2\sigma_m(\mathrm{OMe}) + \sigma_p(\mathrm{OMe}) = -0.03$. Only one Hammett feature was chosen in order to reduce the risk of overfitting in a series of ten analogues [12].

Next, the Hammett-based QSAR model was fitted using ordinary least squares:

$$\overline{\mathrm{pIC}}_{50,i} = \beta_0 + \beta_1\sigma_{\Sigma,i} + \varepsilon_i, \tag{5}$$

where $\overline{\mathrm{pIC}}_{50,i}$ is the mean transformed potency, β_0 is the intercept term, β_1 is the coefficient of the Hammett feature, and ε_i is the residue. The Pearson correlation provided the initial measure of association between the $\sigma_{\Sigma,i}$ value and potency. Subsequently, it was confirmed by the Spearman rank correlation test. Cross-validation with leave-one-out technique ensured the internal reliability of the QSAR:

$$Q^2_{\mathrm{LOO}} = 1 - \frac{\sum_i \left(\overline{\mathrm{pIC}}_{50,i} - \widehat{\overline{\mathrm{pIC}}}_{50,i,-i}\right)^2}{\sum_i \left(\overline{\mathrm{pIC}}_{50,i} - \overline{\overline{\mathrm{pIC}}}_{50}\right)^2}, \tag{6}$$

where $\widehat{\overline{\mathrm{pIC}}}_{50,i,-i}$ represents the fitted response $\mathrm{pIC}_{50,i}$ without including that compound in the training sample, while $\overline{\overline{\mathrm{pIC}}}_{50}$ is the overall average potency in micromolars. In addition, leverage and influential values were inspected to determine whether the association with electronic activation depended on a single compound. Non-parametric bootstrap at the compound level estimated the stability of the linear association. Due to the small number of compounds in the study, statistical results were regarded as chemical hypothesis testing rather than predictive modeling [13, 14, 12].

The Hammett QSAR calls for orthogonal electronic and biological data layers. A quantum chemical descriptor layer consists in optimizing geometry at a dispersion-corrected hybrid density functional with a minimal basis of 6-31+G(d,p) and checking the energy extremality of geometries by vibrational analysis. A polarizable continuum model is recommended for solvent effects with either DMSO or water representing the biological solvent depending on the type of experiment. Key electronic descriptors include HOMO energy, LUMO energy, HOMO-LUMO gap, dipole moment, global electrophilicity index, natural populations or Hirshfeld charges at the beta-carbon, condensed Fukui indices, carbonyl electronegativity, and maximum absolute electrostatic potentials over the enone fragment. According to the hypothesis, potent analogues will exhibit lower LUMO energy, greater electrophilicity indices, and positive charges or electrostatic extrema on the chalcone beta-carbon. Calculated values are not presented, because structures and outputs are not part of the activity data.

The molecular docking technique was used for target ranking rather than mechanism discovery. There are two plausible targets: the first target class relates to topoisomerase II–DNA interactions, whereas the second relates to the tubulin colchicine site, based on known topoisomerase poisoning and antimitotic activity of some chalcones [15, 16]. Targets were selected using the following criteria: protein structure from the PDB database with acceptable resolution, presence of a known co-crystallized ligand, full description of binding sites, and

availability of the co-crystallized ligand. Docking includes preparation of the target structure and co-crystallized ligands, prediction of their protonation state, minimization, redocking of the known ligand, root-mean square deviations check of the docked ligand, repeated docking and interaction fingerprints calculation [17, 18, 19]. Docking scores do not serve as the estimates of the affinity but help to assign a target hypothesis based on the activity profile. A tubulin-mediated mechanism requires docking, G2/M phase arrest, and direct interference with tubulin polymerization. In turn, topoisomerase II-related activity should correlate with inhibition and DNA damage response.

Finally, mechanistically resolving assays allow assigning analogues to the target classes based on the potency and activity spectrum. The focus is made on the analogues contrasting in both the degree and nature of the electronic activation: trimethoxyphenyl analogue 11a, mononitro analogue 11i, dinitro analogues 11j, and fluorine-substituted analogue 11g. Their cytotoxicity is confirmed with A549 and Colo-205 cell lines using 8-10 point sigmoidal concentration–response curves covering and extending above and below IC_{50}. A four-parameter logistic model is used for curve fitting to provide the IC_{50} with confidence intervals and fit statistics. The normal-cell cytotoxicity is determined in at least one normal epithelial line, such as MCF-10A, BEAS-2B, FHC, or ovarian surface epithelial cell line. Selectivity index is calculated as follows:

$$SI = \frac{IC_{50,normal}}{IC_{50,cancer}}. \quad (7)$$

Mechanisms explored with the suite of assays include apoptosis measured by Annexin V/PI double-staining and caspase 3/7 activation in three concentrations, DNA histogram of cell cycle measured via propidium iodide and flow cytometry to determine whether there is a G2/M arrest or apoptosis, ROS formation with DCFH-DA probe and N-acetylcysteine rescue, and glutathione adducts formation with LC–MS to detect Michael-acceptor activity. Other mechanistic assays (topoisomerase II DNA decatenation and tubulin polymerization) are performed if docking results indicate a target involvement. Thus, the assay set distinguishes redox involvement, electrophilic stress, tubulin-related mitosis interference, topoisomerase II binding, and nonspecific mechanisms of cytotoxicity.

Statistical analysis was performed using pIC_{50} measures. The relatively small series was recognized as the key limiting assumption for the hypothesis testing. For this reason, the analysis relied on one electronic descriptor, used Pearson and Spearman correlation analysis, included cross-validation, examined influential observations, did not consider any multi-parameter models, and differentiated between the calculation stage and experimental work. Consequently, the developed QSAR was interpreted as a chemically valid hypothesis rather than as a general predictive model.

3. Results

3.1. Cell-line activity profile

Table 1 provides a brief overview of the curated activity matrix and transformed pIC_{50} values. The pIC_{50} metric facilitates quantitative understanding of the magnitude of the difference in potency between compounds. Compound 11j is the most potent analogue, having pIC_{50} values equal to 7.40 in MCF-7, 8.00 in A549, 6.92 in Colo-205, and 6.82 in A2780. Compound 11i is the next most consistent nitro analogue, while 11a and 11g show balanced low-micromolar activity. Methyl, dimethyl, and dimethylamino analogues show weaker activity, and several entries are unavailable or inactive.

The transformed values are depicted in Figure 1 as a cell-line potency fingerprint, which allows for separation of the maximum potency effect from response breadth. The most potent A549 derivative 11j is still very active in MCF-7 and A2780, but its activity advantage in Colo-205 over etoposide is limited according to the means. Compound 11i shows relatively balanced activity with submicromolar IC_{50}s in each cell line, whereas derivatives 11a and 11g fall between the highly active group centered around 11j and 11i, respectively.

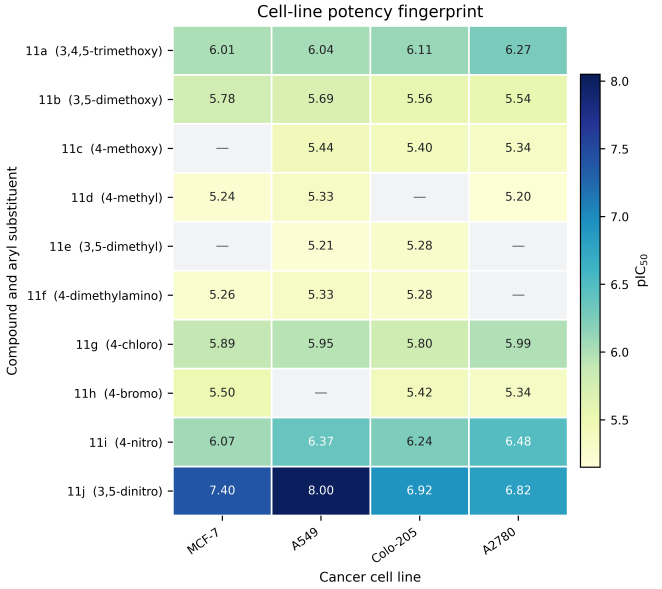

Figure 1: Potency fingerprint for the chalcone series based on transformed pIC_{50} values. The dashes represent missing or inactive entries; the figure highlights diverse response patterns in the same scaffold.

3.2. Relative potency compared to etoposide

Fold-based normalization relative to etoposide produces a clearer interpretation than raw IC_{50} order ranking alone. Compound 11j is 52.8 times more potent than etoposide in MCF-7, 308 times more potent in A549, 8.7 times more potent in A2780, but only 1.08 times more potent in Colo-205. Compound 11i is 2.45, 7.16, and 3.97 times more potent than etoposide in MCF-7, A549, and A2780 cell lines, respectively, but less potent than etoposide in Colo-205. This pattern supports selection of nitro analogues as hits while precluding the overly general conclusion that the entire chalcone series outperforms etoposide in each individual cell line.

3.3. Role of electronic factors in chalcone cytotoxicity

The summary of substituent electronics, mean response, and response dispersion is provided in Table 2. The relationship between substituent electronics and cytotoxic potency is shown in Figure 2. The one-parameter model in Eq. (5) yielded a positive slope of 0.918 pIC_{50}/Hammett units with 76.2% R-squared and explained variance of 0.907. Pearson coefficient of correlation is $r = 0.873$ ($p = 9.84 \times 10^{-4}$); Spearman coefficient is $\rho = 0.796$ ($p = 5.84 \times 10^{-3}$). Bootstrap sampling resulted in a median Pearson coefficient of 0.881 with an approximate 95% interval of 0.378–0.982. Leave-one-out prediction gave a coefficient of determination of $Q^2_{LOO} = 0.510$.

Cell-line-specific correlations also agreed well with the electronic hypothesis. The correlations of $\Sigma\sigma$ with cell-line pIC_{50} are $r = 0.88$ ($p = 0.00434$) for MCF-7, $r = 0.90$ ($p = 0.000947$) for A549, $r = 0.86$ ($p = 0.00318$) for Colo-205, and $r = 0.81$ ($p = 0.0159$) for A2780 (Table 3). These modest-sized but consistent correlations indicate the electronic pattern reproducibility across the cell lines.

Table 1: Curated IC_{50} and transformed pIC_{50} values for compounds 11a–j.

Compound	Aryl substituent	IC_{50} (μM)				Transformed pIC_{50}			
		MCF-7	A549	Colo-205	A2780	MCF-7	A549	Colo-205	A2780
11a	3,4,5-trimethoxy	0.98	0.91	0.78	0.54	6.01	6.04	6.11	6.27
11b	3,5-dimethoxy	1.65	2.03	2.77	2.91	5.78	5.69	5.56	5.54
11c	4-methoxy	–	3.67	3.96	4.56	–	5.44	5.40	5.34
11d	4-methyl	5.82	4.73	–	6.32	5.24	5.33	–	5.20
11e	3,5-dimethyl	–	6.11	5.27	–	–	5.21	5.28	–
11f	4-dimethylamino	5.54	4.68	5.21	–	5.26	5.33	5.28	–
11g	4-chloro	1.29	1.13	1.58	1.03	5.89	5.95	5.80	5.99
11h	4-bromo	3.14	–	3.84	4.56	5.50	–	5.42	5.34
11i	4-nitro	0.86	0.43	0.57	0.33	6.07	6.37	6.24	6.48
11j	3,5-dinitro	0.04	0.01	0.12	0.15	7.40	8.00	6.92	6.82

Dashes indicate inactive, not determined, or absent values. pIC_{50} values were calculated as $6 - \log_{10}(IC_{50,\mu M})$.

Table 2: Summary of electronic effect and potency for the chalcone series.

Compound	Aryl substituent	$\Sigma\sigma$	Mean pIC_{50}	SD of pIC_{50} profile
11a	3,4,5-trimethoxy	-0.03	6.11	0.12
11b	3,5-dimethoxy	0.24	5.64	0.12
11c	4-methoxy	-0.27	5.39	0.05
11d	4-methyl	-0.17	5.25	0.06
11e	3,5-dimethyl	-0.14	5.25	0.05
11f	4-dimethylamino	-0.83	5.29	0.04
11g	4-chloro	0.23	5.91	0.08
11h	4-bromo	0.23	5.42	0.08
11i	4-nitro	0.78	6.29	0.18
11j	3,5-dinitro	1.42	7.29	0.54

$\Sigma\sigma$ is the summed Hammett substituent constant for the aryl substituent pattern. Mean and SD values were computed using active cell-line entries only.

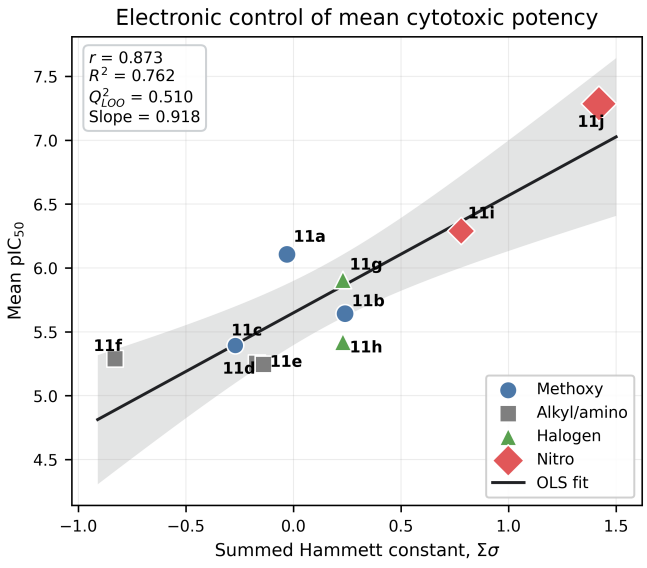

Figure 2: Trend in the mean pIC_{50} versus aryl substituent sum of Hammett constants for the chalcone series. Deviations such as those for 11a and 11j are of key interest for mechanism definition and validation.

3.4. Mechanistic considerations on notable analogues

The electronic trend was clear but partial. For example, 11a had almost neutral electronics by Hammett parameters but showed high cytotoxic activity, especially compared to the closely related 11b and 11c derivatives. This deviation is significant because the 3,4,5-trimethoxyphenyl moiety is known to form part of the active sites in many antimitotic chalcones and colchicine inhibitors [2, 20]. Therefore, compound 11a can be regarded as a defining subseries that activates target recognition through conformational fit rather than purely electronic means.

On the other hand, 11j can also be of special interest due to its unusually strong electronics (dinitro) combined with the highest mean pIC_{50}. Being significantly underpredicted by the one-parameter electronic model in Figure 2, 11j is likely to possess some properties beyond the scope of Hammett electronics, such as enhanced redox cycling, different solubility, ability to produce electrophilic stress, or even non-specific electrophilic reactivity (e.g., DNA alkylation or crosslinking). As such, 11j can be considered a strong probe for further analysis. Compound 11i is a useful comparator as it retains nitro substituents but has a lesser alert profile.

Table 3: Correlations of chalcone cytotoxicity with substituent electronics.

Cell line	Active entries	Pearson r	p value	Spearman ρ	p value
MCF-7	8	0.88	0.00434	0.79	0.0195
A549	9	0.90	0.000947	0.78	0.0125
Colo-205	9	0.86	0.00318	0.82	0.00679
A2780	8	0.81	0.0159	0.75	0.0310

3.5. Evidence map for mechanism discovery and confirmation

The evidence map in Figure 3 connects all the steps required for mechanism definition and confirmation: activity curation, electronic QSAR analysis, DFT descriptors calculation, docking-based target identification and ranking, and selective biological assays. Mechanism was neither deduced from cytotoxicity alone nor from docking alone; instead, it was viewed as the result of convergence between the observed cytotoxic response and chemical characteristics. The proposed mechanism discovery framework is important for separating the unique properties of 11j from the trimethoxyaryl behavior of 11a and electron-withdrawal without nitro substituents in 11g.

4. Discussion

This work revealed that electron-withdrawing aryl substituent is a critical factor in cytotoxic activity of the pyrazolo[1,5-*a*]pyridine–oxadiazole chalcone series. It was established that several compounds from the series were active, with 11j showing the strongest activity [4]. Electron-withdrawing effect provided additional structure to this conclusion by confirming that the chalcone cytotoxicity is increasing as the aryl substituent becomes more electronically demanding. This effect was consistent with the concept of electronic activation of the chalcone acceptor as a critical driver of biological response.

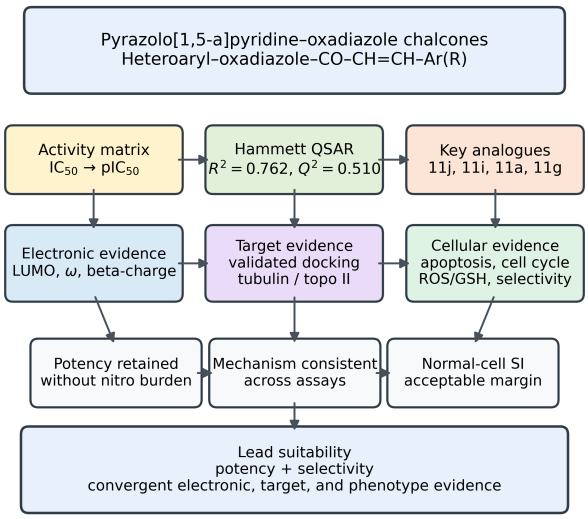

Figure 3: Proposed mechanism-resolving evidence map for the chalcone series. It includes activity transformation, electronic QSAR, DFT descriptors, target docking and scoring, cell-type-selective assays, and other steps required for mechanism elucidation and confirmation.

While the effect of electron-withdrawing substituents was strong, it does not imply that increasing electron withdrawing power enhances the medicinal potential. On the contrary, the dinitro substituent in compound 11j makes it an effective probe of the cytotoxic response but not necessarily a good lead. For example, dinitro compounds can cause mutagenesis [10, 11]. Compound 11j is a potent chalcone but is unsuitable until the selectivity and underlying mechanism are known. Compound 11i provides a valuable comparative probe due to its mononitro substituents that retain strong activity. Compound 11a remains important due to the trimethoxyaryl motif which might suggest some antimitotic activity. Compound 11g allows comparing non-nitro, electron-withdrawing derivatives to nitro derivatives.

These suggestions follow directly from limitations of cytotoxicity-only analysis and call for additional assays that allow discrimination between selective cytotoxicity and metabolic effects such as interference, solubility effects, mitochondrial dysfunction, etc. The proposed activity profiling assay set would distinguish selective mechanisms (e.g., topoisomerase inhibition) from broad metabolic interference. It includes repeated measurement of dose–response with multiple concentrations and controls, apoptosis, cell-cycle profile and G2/M accumulation, ROS/glutathione metabolism testing, and target-specific assays such as topoisomerase II or tubulin inhibition.

The DFT analysis is the computational component complementing the Hammett electronics analysis. Assuming the validity of the correlation shown in Figure 2, one expects that active compounds 11i and 11j would have low LUMO energies and high global electrophilicity index. Moreover, active compounds 11i, 11j should have increased acceptor property of the beta carbon. On the other hand, if the electronic QSAR did not apply, DFT could help understand what distinguishes active analogues from inactive analogues beyond their electronics.

Similarly, docking should not be interpreted as the evidence of biological response and mechanism. While docking provides hypotheses about plausible targets, docking scores are not sufficient to establish mechanism. The docking procedure has to be validated by redocking, followed by interaction fingerprint comparison and consistency with experimental data (e.g., apoptosis, ROS, tubulin inhibition, etc.). In case of the trimethoxy derivative 11a, G2/M phase arrest and tubulin binding become critical. For nitro derivatives 11i and 11j, topoisomerase II inhibition should be the most important. ROS rescue would point to electrophilic stress mechanism in 11i and 11j.

It was assumed that with only ten molecules in the dataset, a multi-parameter QSAR might be overfit. The one-parameter electronic model was therefore limited in scope but robust enough (with internal $Q^2_{\mathrm{LOO}} = 0.510$) to confirm the substituent effect and provide the basis for further research. Further, the model should be validated and expanded by generation of novel derivatives. Such new derivatives should substitute nitro groups with other electron-withdrawing moieties (e.g., cyano, trifluoromethyl, sulfinyl, sulfonyl, etc.) and determine whether the nitro substituent plays a critical role or not.

5. Implications for next-generation analogue design

Several suggestions can be made based on the obtained results. First, 11j is a promising molecule for further mechanism probing but is too extreme in terms of substituent electronics to use as a lead. Second, 11i has a reasonable substituent electronics while retaining the nitro substituent and therefore provides the optimal balance. Third, 11a shows activity and represents an interesting direction for further antimitotic investigation. Fourth, halogenated or non-nitro electron-withdrawing analogues are needed to decouple substituent effect from nitro substitution. Such analogues include, in particular, 4-cyano, 3,5-dicyano, 4-trifluoromethyl, 3,5-bis(trifluoromethyl), 4-sulfonyl, and others.

6. Conclusions

The pyrazolo[1,5-*a*]pyridine–1,3,4-oxadiazole chalcone scaffold possesses an unambiguous electronic feature which cannot be identified by IC_{50} ordering alone. Activity matrix analysis confirms that electron-withdrawing aryl substituents show a correlation with increased toxicity, which is consistent with the electronic effect on activation of the acceptor chalcone moiety. While compound 11j is the most active derivative, its presence of two nitro groups means that selectivity, redox property, electrophilicity and binding to biological target need to be directly evaluated before declaring it as a potential lead. Nitro effect-driven activation, target hypothesis with trimethoxy aryl derivatives and electronic effect without nitro groups can be clearly distinguished using compounds 11i, 11a and 11g, respectively. DFT descriptor, docking validation, apoptosis assay, cell cycle, ROS/glutathione assay, topoisomerase II inhibition, tubulin polymerization and normal cell selectivity experiments will be useful in this direction.

References

[1] Go, M. L., Wu, X., & Liu, X. L. (2005). Chalcones: An update on cytotoxic and chemoprotective properties. *Current Medicinal Chemistry*, *12*, 483–499.
[2] Ducki, S., Forrest, R., Hadfield, J. A., Kendall, A., Lawrence, N. J., McGown, A. T., & Rennison, D. (1998). Potent antimitotic and cell growth inhibitory properties of substituted chalcones. *Bioorganic & Medicinal Chemistry Letters*, *8*, 1051–1056.
[3] Dimmock, J. R., Kandepu, N. M., Quail, J. W., Pugazhenthi, U., Sudom, A. M., Chamankhah, M., & Balzarini, J. (1998). Cytotoxic 1,3-diaryl-2-propen-1-ones and related compounds. *Journal of Medicinal Chemistry*, *41*, 1014–1026.
[4] Alapati, K. B., Sravani, D., Sailaja, B. B. V., Saritha, B., & Nalla, S. (2026). Design, synthesis, and anticancer activity of chalcone derivatives of pyrazolo[1,5-*a*]pyridine-1,3,4-oxadiazole. *Chemical Data Collections*, *61*, 101214.
[5] Hammett, L. P. (1937). The effect of structure upon the reactions of organic compounds: Benzene derivatives. *Journal of the American Chemical Society*, *59*, 96–103.
[6] Hansch, C., & Fujita, T. (1964). ρ-σ-π analysis: A method for the correlation of biological activity and chemical structure. *Journal of the American Chemical Society*, *86*, 1616–1626.
[7] Becke, A. D. (1993). Density-functional thermochemistry. III. The role of exact exchange. *Journal of Chemical Physics*, *98*, 5648–5652.
[8] Lee, C., Yang, W., & Parr, R. G. (1988). Development of the Colle–Salvetti correlation-energy formula into a functional of the electron density. *Physical Review B*, *37*, 785–789.

[9] Parr, R. G., von Szentpaly, L., & Liu, S. (1999). Electrophilicity index. *Journal of the American Chemical Society*, *121*, 1922–1924.
[10] Baell, J. B., & Holloway, G. A. (2010). New substructure filters for removal of pan assay interference compounds (PAINS) from screening libraries and for their exclusion in bioassays. *Journal of Medicinal Chemistry*, *53*, 2719–2740.
[11] Nepali, K., Lee, H. Y., & Liou, J. P. (2019). Nitro-group-containing drugs. *Journal of Medicinal Chemistry*, *62*, 2851–2893.
[12] Dearden, J. C., Cronin, M. T. D., & Kaiser, K. L. E. (2009). How not to develop a quantitative structure–activity or structure–property relationship (QSAR/QSPR). *SAR and QSAR in Environmental Research*, *20*, 241–266.
[13] Gramatica, P. (2007). Principles of QSAR model validation: Internal and external. *QSAR & Combinatorial Science*, *26*, 694–701.
[14] Tropsha, A. (2010). Best practices for QSAR model development, validation, and exploitation. *Molecular Informatics*, *29*, 476–488.
[15] Nitiss, J. L. (2009). Targeting DNA topoisomerase II in cancer chemotherapy. *Nature Reviews Cancer*, *9*, 338–350.
[16] Pommier, Y., Leo, E., Zhang, H., & Marchand, C. (2010). DNA topoisomerases and their poisoning by anticancer and antibacterial drugs. *Chemistry & Biology*, *17*, 421–433.
[17] Morris, G. M., Huey, R., Lindstrom, W., Sanner, M. F., Belew, R. K., Goodsell, D. S., & Olson, A. J. (2009). AutoDock4 and AutoDockTools4: Automated docking with selective receptor flexibility. *Journal of Computational Chemistry*, *30*, 2785–2791.
[18] Trott, O., & Olson, A. J. (2010). AutoDock Vina: Improving the speed and accuracy of docking with a new scoring function, efficient optimization, and multithreading. *Journal of Computational Chemistry*, *31*, 455–461.
[19] Warren, G. L., Andrews, C. W., Capelli, A.-M., Clarke, B., LaLonde, J., Lambert, M. H., Lindvall, M., Nevins, N., Semus, S. F., Senger, S., Tedesco, G., Wall, I. D., Woolven, J. M., Peishoff, C. E., & Head, M. S. (2006). A critical assessment of docking programs and scoring functions. *Journal of Medicinal Chemistry*, *49*, 5912–5931.
[20] Jordan, M. A., & Wilson, L. (2004). Microtubules as a target for anticancer drugs. *Nature Reviews Cancer*, *4*, 253–265.